Contents lists available at ScienceDirect

Journal of Hydrology

journal homepage: www.elsevier.com

Research papers

Estimating anisotropic heterogeneous hydraulic conductivity and dispersivity in a layered coastal aquifer of Dakshina Kannada District, Karnataka

B.N. Priyanka[a], M.S. Mohan Kumar[a, b, *], Mahesha Amai[c]

[a] Department of Civil Engineering, Indian Institute of Science, Bengaluru 560 012, India
[b] ICWaR and Indo-French Cell for Water Sciences, Indian Institute of Science, Bengaluru 560 012, India
[c] Department of Applied Mechanics and Hydraulics, National Institute of Technology, Karnataka Surathkal, Mangalore 575 025, India

ARTICLE INFO

This manuscript was handled by P. Kitanidis, Editor-in-Chief, with the assistance of Chunhui Lu, Associate Editor

Keywords:
Seawater intrusion
Parameter estimation
Dispersivity
Hydraulic conductivity
Pilot point

ABSTRACT

The solution for the inverse problem of seawater intrusion at an aquifer scale has not been studied as extensively as forward modeling, because of the conceptual and computational difficulties involved. A three-dimensional variable-density conceptual phreatic model is developed by constraining with real-field data such as layering, aquifer bottom topography and appropriate initial conditions. The initial aquifer parameters are layered heterogeneous and spatially homogeneous that are based on discrete field measurements. The developed conceptual model shows poor correlation with observed state variables (hydraulic head and solute concentration), signifying the importance of spatial heterogeneity in hydraulic conductivity and dispersivity of all the layers. The conceptual model is inverted to estimate the anisotropic spatially varying hydraulic conductivity and the longitudinal dispersivity at the pilot points by minimizing the least square error of state variables across the observation wells. The inverse calibrated model is validated for the hydraulic head at validation wells and the solute concentration is validated with equivalent solute concentration derived from the electrical resistivity, which shows good results against the field measurements. The verification of estimated anisotropic hydraulic conductivity with the electrical resistivity tomography image shows good agreement. This investigation gives an insight about constraining the highly parameterized inverse model with real-field data to estimate spatially varying aquifer parameters for an effective simulation of the seawater intrusion in a layered coastal aquifer.

1. Introduction

Aquifer characterization is one of the important input in groundwater simulation models. The information about the aquifer characteristics is usually determined by conducting field experiments such as pumping test, electrical resistivity, borehole logging, etc. But, conducting field experiments to determine the aquifer parameters for the entire study area is not feasible.

An inverse approach is a standard tool used for the parameter estimation in the subsurface hydrology. There are mainly two methods to estimate parameters, i.e., deterministic approach and geostatistical approach. In a deterministic approach, the geological information in terms of spatial variability/zonation can be incorporated in the model. The main disadvantage of the deterministic models is its inability to estimate the uncertainty, but are reliable for predicting SWI and have much greater robustness for incorporating the concentrations data for estimating the aquifer parameters (Pool et al., 2015). The geostatistical approach considers the parameters such as random field and assumes that the spatial variability is unknown. The stochastic approaches can address uncertainties well and can give better results. But the stochastic models perform poorly and underestimates uncertainty when the data given is scanty (Pool et al., 2015). Hence, in the present investigation, a deterministic inverse approach is used.

In the past, an inverse approach was extensively used to estimate the groundwater flow parameters (e.g., Emsellem and De Marsily, 1971; Frind and Pinder, 1973; Cooley, 1977; Kitanidis and Vomvoris, 1983; Carrera 1988; McLaughlin and Townley, 1996; Franssen and Gómez-Hernández, 2002; Franssen et al., 2009; Pool et al., 2015), while the inverse approach to estimate/identify the solute transport parameters received little attention (e.g., Murty and Scott, 1977; Umari et al., 1979; Giacobbo et al., 2002; Bray et al., 2007). From the late 1980′s, considerable research has been carried out to estimate both flow and solute transport parameters. Strecker and Chu (1986) and

* Corresponding author at: Department of Civil Engineering, Indian Institute of Science, Bengaluru 560 012, India.
Email address: msmk@iisc.ac.in (M.S. Mohan Kumar)

https://doi.org/10.1016/j.jhydrol.2018.08.031
Received 10 January 2018; Received in revised form 6 August 2018; Accepted 13 August 2018
Available online xxx
0022-1694/

Keidser and Rosbjerg (1991) estimated the groundwater flow and transport parameters separately in two stages, but these approaches cannot be used to solve the coupled inverse problem. Considerable research has been carried out to estimate both groundwater flow and transport parameters simultaneously (e.g., Wagner and Gorelick, 1986; Wagner, 1992; Xiang et al., 1992; Medina and Carrera, 1996; Mayer and Huang, 1999; Sun et al., 2001; Franssen et al., 2003; Sanz and Voss, 2006; Bastani et al., 2010). Most of the proposed methods were applied to hypothetical/synthetic aquifers and limited work has been carried out on three-dimensional (3D), variable-density, inverse modeling at an aquifer scale (e.g., Medina and Carrera, 1996; Mayer and Huang, 1999; Bastani et al., 2010; Dausman et al., 2010; Ataie-Ashtiani et al., 2013). The real-field coupled inverse problem may be ill-posed if they are solved considering the state variables only and without any information on the parameters to be estimated. The use of prior information in the optimization process will improve the identification of heterogeneity (Alcolea et al., 2006), remove the non-uniqueness and provide stability to the solutions.

The parameter estimation for the 3D real-field problems such as seawater intrusion (SWI) in a coastal aquifer is a complex and dynamic problem. In the past, modelers have estimated the flow and solute transport parameters for the SWI problems. Iribar et al. (1997), estimated the transmissivity values by considering the piezometric head and the chloride concentration in a confined aquifer of Llobregat Delta. For the same aquifer, Abarca et al. (2006) estimated zonal aquifer heterogeneity for a 2D horizontal groundwater flow and solute transport model. In both the studies, the density effects were neglected since the aquifer thickness and the elevation gradients were small. The density effect was studied by Sanz and Voss (2006) to estimate the flow and transport parameters but on a standard Henry problem. Bray et al. (2007) estimated the flow and solute transport parameters in a 3D variable-density conceptual model but in two independent and successive phases. This method is not a coupled flow and solute transport inversion. The inverse modeling of a 3D variable-density groundwater flow and solute transport system was carried out by Dausman et al. (2010). They addressed the computational complexities involved in the inverse modeling, but the plume migration pathways were based on multiple hypotheses. Beaujean et al. (2014) used the solute concentration values as a state variable which were derived from the electrical resistivity tomography to estimate parameters in a 2D model.

A number of studies have been carried out on the inverse modeling in a 3D coastal aquifer considering the density effect and field measurements (e.g., Bastani et al., 2010; Ataie-Ashtiani et al., 2013; Lathashri and Mahesha, 2015) but the aquifer parameters estimated were either isotropic or homogeneous. The literature survey confirms that not many studies have been carried out to the estimate anisotropic spatially varying aquifer parameters in a 3D conceptual model, because of the significant computational resources and the time required. The computational and conceptual difficulties in the parameter estimation for a 3D variable-density coupled groundwater flow and solute transport in the coastal aquifers were reviewed by Carrera et al. (2010). They have reviewed in detail on these computational and conceptual issues. Ketabchi and Ataie-Ashtiani (2015) have discussed the computational problems involved in solving the simulation-optimization framework and how to resolve them. Rajabi and Ketabchi (2017) have addressed the computational challenge in solving a simulation-optimization framework by employing Gaussian process emulation in Kish Island, Persian Gulf.

The present study focuses on considering the conceptual issues such as layering, aquifer bottom topography, and appropriate initial field conditions to estimate the parameters in a coastal aquifer. The objectives of the paper are (1) estimating anisotropic hydraulic conductivity and longitudinal dispersivity; (2) developing a reliable validation method to evaluate numerical model results with electrical resistivity tomography (ERT); (3) verifying the estimated anisotropic hydraulic conductivity with ERT images. The analysis gives an insight into the layering, anisotropic and heterogeneity constraint to simulate the groundwater flow and SWI phenomenon at an aquifer scale and a comprehension about the geological formation of the region. Thus, this investigation will be useful for the analysis of SWI inversion problem at an aquifer scale.

2. Description of study area

The study area falls under the Surathkal and Mukka region of Dakshina Kannada District, Karnataka located along the west coast of India (Fig. 1a). The aerial extent is about 8 km^2 and the area is surrounded by the Arabian Sea on the west and the seasonal tidal River Pavanje in the north and north-eastern part (Fig. 1b). The area is characterized by relatively undulating terrain with altitudes ranging up to 37 m above Mean Sea Level (MSL). The coastal and the Pavanje River length in the study area are around 3.1 km and 5.5 km, respectively. The terrain is relatively flat near the coast causing SWI into the river for several kilometers thus, contaminating the adjacent freshwater aquifer. Since Pavanje is a non-perennial river, the water required for the agriculture and domestic use is mainly met by groundwater during the non-monsoon period. This region falls under a tropical humid climate with an annual average rainfall of about 3797 mm and approximately 87% of which is experienced from June–September.

There are 14 observation wells considered in the area which are well spread with one observation well for 1 km^2; except for the south-western part which is barren. The water level and quality in these wells were monitored once in a month over a period of three years from 2005 to 2008 (Vyshali, 2008).

The IRD (Institut de Recherche pour le Développement, France) and NITK (National Institute of Technology Karnataka, Surathkal) conducted 2D electrical resistivity test, borehole logging (Fig. 1c) and pumping tests to delineate the geological formation and to characterize the aquifer in this region. The electrical resistivity test was carried out using Wenner Alpha and Beta arrays together with an inter-electrode spacing of 4 m and data inversion was performed using Res2dInv software (Geotomo Software). The robust inversion method adopted gave good results with an absolute error of $<5\%$ (Hoareau, 2009). Hoareau (2009) combined interpretation of inverted electrical resistivity measurements and information derived from the borehole logging (such as magnetic susceptibility, groundwater resistivity, rock apparent resistivity, etc.) to establish a relationship between the ranges of electrical resistivity tomography (ERT) and geological formations (Table 1). The Vertical Electrical Soundings (VES) carried out by Mahesha et al. (2012) near the observation wells gives information on the geological formation (Table 1) and the layer thickness.

Based on the available borehole logging details (Fig. 2), ERT and VES results, it can be inferred that the soil composition of the aquifer layers is as follows:

Layers 1 and 2 (i.e., Ground Level (GL) to 20 m thick layer of coastal alluvium) consists of clayey soil, clayey sand, fine silt and lateritic clay. The top surface of the soil is hard and red in color. The porosity of these layers varies between 0.25 and 0.6 (Udayakumar, 2008). The hydraulic conductivity for the clay and silt formation varies between 0.35 and 10 m/d (Freeze and Cherry, 1979) and for the lateritic clay it is between 10 and 30 m/d (Bhosale and Kumar, 2001).

Layers 3 and 4 (i.e., GL to 30 m thick layer of the weathered zone and weathered zone with clay formation). This layer is formed due to weathering of crystalline or sedimentary rocks. The porosity and hydraulic conductivity vary between 0.2 and 0.3 and 25–70 m/d (Bhosale and Kumar, 2001), respectively.

A layer of fissured zones with sequences of highly fissured bedrock can be seen in between the layers of the coastal alluvium and the

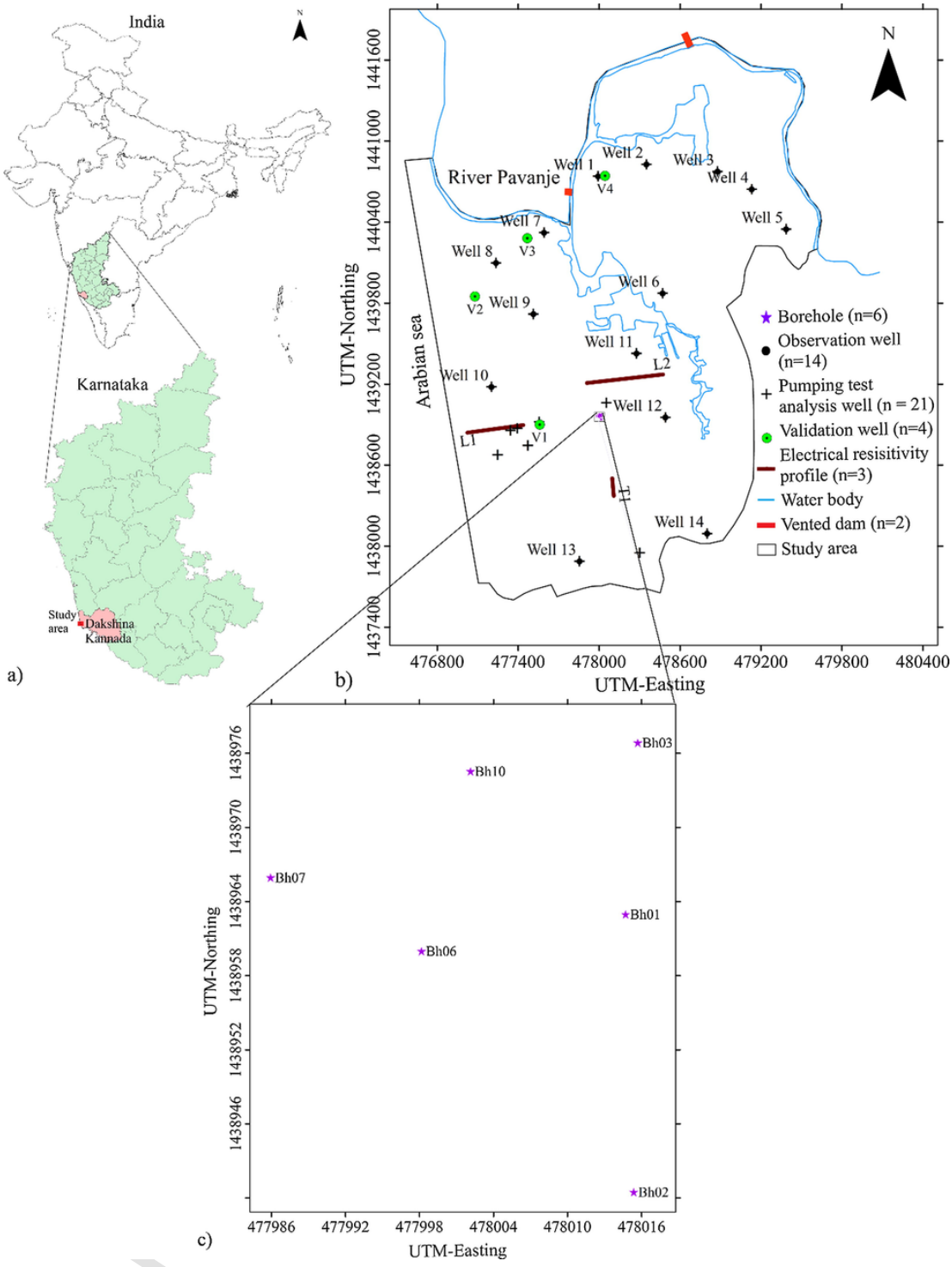

Fig. 1. (a) The study area is located on the west coast of Karnataka, India, (b) study area with the location of boreholes, observations wells, pumping test wells, validation wells, resistivity profile and vented dams, and (c) location of the boreholes.

weathered zone (Fig. 2). The porosity and hydraulic conductivity vary between 0.05 and 0.3 and 5–30 m/d (Freeze and Cherry, 1979), respectively.

Layer 5: Deeper down, the fresh bedrock with relatively less fissures is present.

3. Model development and inputs

3.1. Description of the numerical model

To simulate the transient variable-density groundwater flow and solute transport, a finite element numerical code FEFLOW (Finite Element Modeling of FLOW, mass and heat transport in porous and frac-

Table 1
Interpretation of resistivities from the electrical resistivity and VES test.

Resistivities	Interpretation of resistivity test (Hoareau, 2009; Mahesha et al., 2012)	Hydraulic conductivity values
<30O-m	Saturated sand/clay formation with intruded seawater	0.35–5 m/d
30–80O-m	Clayey sand or fine silt	0.35–5 m/d
80–400O-m	Weathered zone	25–70 m/d
400–800O-m	Fissured zone	5–30 m/d
800–10,00O-m	Poorly fissured zone	5–30 m/d
>10,00O-m	No factures/bedrock	–

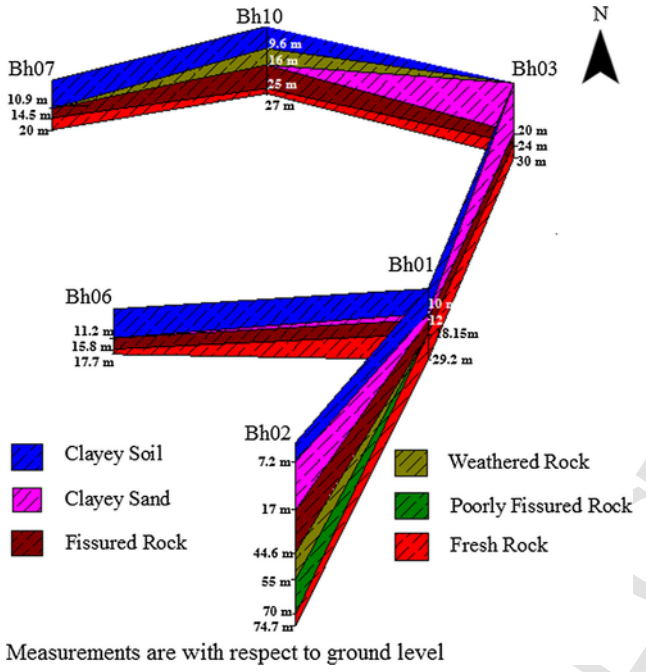

Fig. 2. Fence diagram from borehole logging.

tured media) version 7.0.9x (WASY GmbH, Berlin, Germany, 2016) is used. This numerical code was developed by Hans-Jörg G. Diersch in late 1970′s and is one of the widely used code in modeling of SWI (e.g., Kopsiaftis et al., 2009; Sherif et al., 2012; Lu et al., 2013). The FEFLOW code is validated on standard benchmark problems such as Henry, Elder, and salt dome (Kolditz et al., 1998). The flow and solute transport equation is given as (Diersch, 2014)

$$\left(S_s B + S_y\right)\frac{\partial h}{\partial t} + \nabla.(\bar{q}) = Q \tag{1}$$

$$\frac{\partial(\varepsilon C)}{\partial t} + \nabla.(\bar{q}C) - \nabla.\left(\bar{D}.\nabla C\right) = QC \tag{2}$$

where, $\bar{q} = -\mathrm{K}Bf_{\mu}.\nabla h$ (Darcy equation); S_s = specific storage [L^{-1}]; B = thickness of saturated phreatic aquifer [L]; S_y = specific yield; ε = effective porosity; K = hydraulic conductivity tensor [LT^{-1}]; f_{μ} = μ_0/μ = viscosity relation function, $h = z + (p/\gamma)$ = hydraulic head [L]; z = datum head [L]; p = fluid pressure [$ML^{-1}T^{-2}$]; γ = specific weight of fluid [$ML^{-1}T^{-2}$]; Q = volumetric flow rate of source/sink term [T^{-1}]; C = solute concentration; $\bar{D} = \varepsilon BD_m\delta + D$; D_m = molecular diffusion coefficient [L^2T^{-1}]; δ = identity tensor; D = mechanical dispersion tensor [L^2T^{-1}].

The Galerkin finite element numerical method with no up-winding is used for the transient simulation. Here, 3D triangular meshes are generated by using triangulation, Picard iteration method is used to treat the nonlinearities, and the matrices are solved by the conjugate gradient methods. The second order accurate explicit Adams–Bashforth predictor and trapezoidal rule corrector method (AB/TR) is used for time stepping. For further details on FEFLOW, the reader can refer to Diersch (2014).

3.1.1. Aquifer topography and discretization

A 3D unconfined conceptual model is developed with its origin at 4,76,559.78 m Easting and 14,37,602.16 m Northing as per World Geodetic System (WGS) 84/Universal Transverse Mercator (UTM) zone 43N in the horizontal plane. The vertical section of the 3D model is represented by 5 layers (Fig. 3a) and the thickness of each layer is shown in Fig. 3b. The axis normal to the sea is x, an axis parallel to the sea is y and along the depth, the axis is z. The polygonal area is proposed with a total number of 249,140 elements (i.e., 49,828 elements in each layer) and 159,492 nodes. The proposed mesh is refined at the analysis wells and along the boundary of the region (Fig. 3c). The Shuttle Radar Topography Mission (SRTM) of 1 arc-second data is interpolated to get the top elevation at the nodal points. The surface elevation varies between 0 and 37 m above MSL and the bottom topography of the aquifer varies from −42 m (below MSL) to about 6 m (above MSL). Based on the depth of the observation wells, borehole logging, and VES data, the thickness of each layer is assigned and interpolated for the entire model.

3.2. Description of the inverse code

The output error criterion is used for the parameter estimation; here, the difference between the observed and simulated state variables at the observation points are minimized. The nonlinear PEST (model-independent Parameter ESTimation) developed by John Doherty (1994), is used as an inverse code. PEST runs the FEFLOW iteratively by adjusting the values of parameters to be estimated until the errors between the observed and simulated state variables reach the terminating criterion. The Gauss–Levenberg–Marquardt algorithm (GLMA) is used for minimizing the objective function, Eq. (3)

$$\text{minimize}\ \Phi_o = w_{hi}\sum_{i=1}^{m}\left\{\sum_{t=1}^{n}\left(\left[h_t\right]_i - \left[h_t^*\right]_i\right)^2\right\} + w_{Ci}\sum_{i=1}^{m}\left\{\sum_{t=1}^{n}\left(\left[C_t\right]_i - \left[C_t^*\right]_i\right)^2\right\} \tag{3}$$

$$\text{constraint}\ p_j^l \leqslant p_j \leqslant p_j^u \tag{3a}$$

where, i = 1, 2, ……..., m = number of observation wells; t = observed time interval = 1, 2,....., n; h^* and C^* are hydraulic head and solute concentration vectors, respectively, at the observation points; h and C are computed hydraulic head and solute concentration vectors, respectively; w is the associated weight; p is the parameter to be estimated; l and u are lower and upper bounds of the parameters, respectively, which are obtained from the geological information (Table 1) and j is a node. The observation weights are computed from the reciprocal of the standard deviation (σ) of measurements. The weights for the hydraulic head varies between 0.67 and 1.25 and for solute concentration, weight varies between 0.01 and 0.1. The higher weight of 1 is assigned for the solute concentration data of the wells 7 and 11 since these wells are used for the model evaluation.

Tikhonov regularization and singular value decomposition are used to prevent numerical instability and non-uniqueness while estimating a large number of parameters. For further details on mathematical regularization in PEST, the reader can refer to Doherty (2004). Anyone of the following criterion can be used to terminate the iterative process.

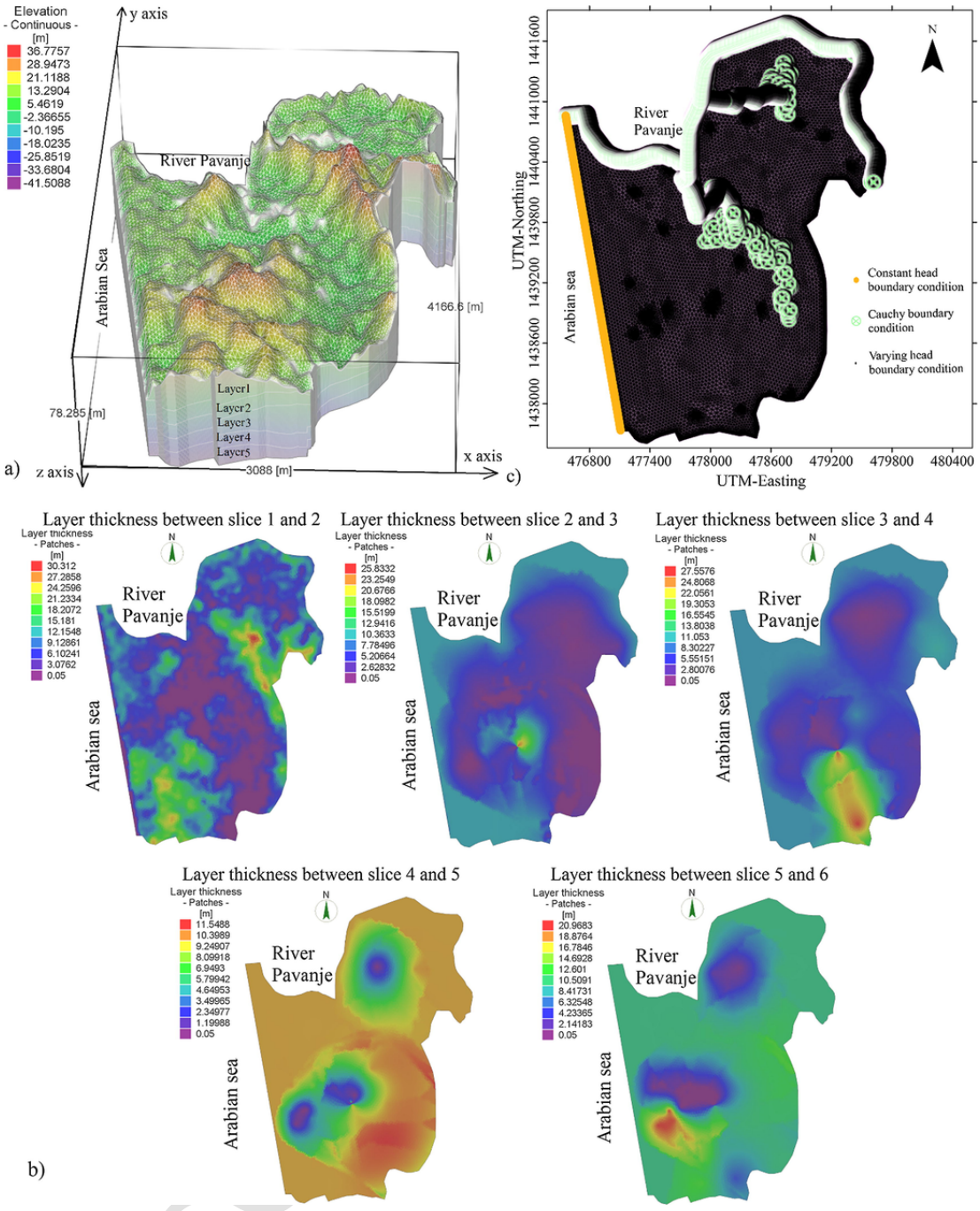

Fig. 3. Conceptual model (a) 3D model, (b) thickness of the layer in between the slices, and (c) aerial view with boundary conditions.

- If $\Phi_i \leq 0.25$, where Φ_i = the objective function value at the end of the i^{th} optimization iteration
- If the maximum number of optimization iterations are 30.
- If $\frac{\Phi_i - \Phi_{min}}{\Phi_i} \leqslant 0.1$, where Φ_{min} = the lowest objective function achieved till time.
- If $\frac{p_{i-1} - p_i}{p_{i-1}} \leqslant 0.1$, relative change in parameter p between optimization iterations $i-1$ and i.

3.3. Model inputs

3.3.1. Boundary and initial conditions

Dirichlet boundary condition:

$$\text{Coast}: h(x,t) = h_{\text{equi}} \text{ on } R_1 \times t\,[t_0, t] \tag{4}$$

$$C(x,t) = C_D \text{ on } R_1 \times t\,[t_0, t] \tag{5}$$

$$\text{Other part}: h(x,t) = h_D(t) \text{ on } R_2 \times t\,[t_0, t] \tag{6}$$

Cauchy boundary condition:

$$\text{River}: q_h(x,t) = -\Phi_h\left(h_C(t) - -h(t)\right) \text{ on } R_3 \times t\left[t_0, t\right] \quad (7)$$

$$\text{where } \Phi_h = \left\{ \begin{matrix} \Phi_h^{in} \text{ for } h_C > h \\ \Phi_h^{out} \text{ for } h_C \leqslant h \end{matrix} \right\} \quad \text{and } \Phi_h = \frac{K}{d} \quad (7a)$$

$$q_C(x,t) = -\Phi_C\left(C_C(t) - -C(t)\right) \text{ on } R_3 \times t\left[t_0, t\right] \quad (8)$$

$$\text{where } \Phi_C = \left\{ \begin{matrix} \Phi_C^{in}(x,t) \text{ for } C_C > C \\ \Phi_C^{out}(x,t) \text{ for } C_C \leqslant C \end{matrix} \right\} \quad \text{and } \Phi_C = -q_h \quad (8a)$$

where, h = hydraulic head [L]; C = solute concentration [ML^{-3}]; t_0 = initial time [T]; R_1 = coastal boundary; h_{equi} = equivalent freshwater head [L]; C_D = solute concentration along the coastal line [ML^{-3}]; R_2 = other boundary; $h_D(t)$ = specified head [L]; R_3 = river boundary; q_h = boundary flux [L^2T^{-1}]; Φ_h = transfer coefficient [T^{-1}]; K = hydraulic conductivity of river bed material [LT^{-1}]; d = river bed thickness; h_C = reference hydraulic head from river stage [L]; q_C = boundary mass flux [$ML^{-2}T^{-1}$]; Φ_C = mass transfer coefficient [LT^{-1}].

The coastline (R1) is defined as a Dirichlet boundary condition as shown in Fig. 3c. The hydraulic head is prescribed as an equivalent freshwater head over full thickness, i.e., 41 m (Motz and Sedighi, 2009). The solute concentration of the seawater is normally estimated based on the Total Dissolved Solids (TDS) (e.g., Cobaner et al., 2012; Sherif et al., 2012; Ding et al., 2014). Therefore, the solute concentration of seawater along the coastal line is given a TDS value of 35 kg/m^3. The river boundary (R3) is defined as a Cauchy boundary condition, which accounts for the flow between the River Pavanje and groundwater system. The data of the river stage, hydraulic conductivity of the river bed material (K) and thickness of the river bed (d) are required to prescribe this boundary condition. The monthly river stage is obtained from the Minor Irrigation Department and the Water Resources Information System of India. The hydraulic conductivity of Pavanje River bed is 7.85 m/d (Sujay and Deka, 2016) and the thickness of the river bed is assumed as 0.8 m, which are fixed for the entire length of the river. The solute concentration (referred to as TDS in the study) of the river varies due to the mixing of freshwater and seawater. The solute concentration in the river is considered only till second vented dam (Fig. 1b) which is 3.32 km along river length from the coastal line, beyond this point C = 0 mg/L. For region R_2, as there is no natural boundary condition, specified head (from hydraulic head contour) and specified concentration (from solute concentration contour) are used. The top boundary condition is defined as a specified flux (recharge rate), which is phreatic in nature. The bottom boundary is considered as a no-flow boundary condition. The initial hydraulic head for the domain is assigned for the starting month (i.e., for February 2005) at discrete observation points and Kriging (e.g., Yao et al., 2014; Xiao et al., 2016) is used to get the continuous hydraulic head. The initial solute concentration/mass concentration is assigned with steady-state simulation output integrated with the observation data points.

3.3.2. Source and sinks

The main source and sink for groundwater in the study area are recharge and groundwater draft, respectively. During the monsoon period (June–September), the aquifer is replenished to the saturation level. The rainfall is the main source for aquifer recharge but during the non-monsoon period, the Pavanje River contributes. The recharge is computed by multiplying the recharge coefficient with monthly rainfall data (IMD, 2004–2010 data). Udayakumar (2008) estimated the appropriate recharge coefficient values, which is in the range of 8–26.5% but according to the Groundwater Estimation committee (GEC, 1997), for the west coast of India, recharge coefficient can be considered in the range of 8–12%. Therefore, in the present investigation, the recharge coefficient is considered to be 10%. As the study area is small, a uniform recharge rate is assumed throughout the layer 1. There are 374 pumping wells in the region, which contributes as the main sink (Lathashri and Mahesha, 2015). The freshwater draft data for pre-monsoon, monsoon and post-monsoon from these 374 wells are taken from Lathashri and Mahesha (2015). The subsurface discharge to the sea and the river are the other sinks which are considered in boundary conditions.

3.3.3. Initial aquifer parameters

The aquifer parameters, i.e., transmissivity and specific yield estimated by Mahesha et al. (2012) using the pumping test at discrete points are interpolated using Kriging in the present study to get the hydraulic conductivity and specific yield for the first layer as shown in Fig. 4a and b, respectively. The arithmetic mean (μ) and standard deviation (σ) of the spatially varying hydraulic conductivities are 11.882 m/d and 4.84 m/d, respectively, and for a specific yield μ = 0.086 and σ = 0.065. Since most of the wells are shallow (3 to 11 m), the pumping test is restricted to the top layer of the developed conceptual model. Based on the pumping test results (Mahesha et al., 2012), the hydraulic conductivity value of layer 1 is found to be spatially varying (Fig. 4a) and transversely isotropic i.e., $K_{xx} = K_{yy} \neq K_{zz}$. The hydraulic conductivity of the remaining layers is considered as layered heterogeneous based on the soil type (Table 1). Based on the earlier investigations in the study area such as borehole logging, VES and pumping test (Udayakumar 2008; Hoareau, 2009; Mahesha et al., 2012) and other studies (Freeze and Cherry, 1979; GEC, 1997; Lathashri and Mahesha, 2015), layer-wise input values for flow and solute transport parameters are as in Table 2. The vertical hydraulic conductivity value is assumed to be 10% of horizontal hydraulic conductivity in the x major axis from layer 3 onwards.

There are no field measurements of dispersivity values of the study area. The longitudinal dispersivity (α_L) values are determined by using the regression formula derived previously to relate the field scale length and dispersivity. In the present investigation, a statistical model using the available data with varying reliabilities derived by Xu and Eckstein (1995) is used to estimate the α_L values. The equation is given by:

$$\alpha_L = 0.83\left(\log_{10} L\right)^{2.414} \quad (9)$$

where L = field scale, m; α_L = longitudinal dispersivity, m; low reliable data = weight 1; intermediate reliable data = weight 2 and high reliable data = weight 3; and Eq. (9) is valid for field scale up to 1 km. But for the conceptual model developed, Eq. (9) is assumed to be valid beyond 1 km. The transverse dispersity (α_T) is considered to be 1/10th of longitudinal dispersivity (e.g., Cobaner et al., 2012; Lathashri and Mahesha, 2015). The spatial distribution α_L is same in all the layers (Fig. 5). The other parameters considered are uniform for all the layers (Table 3). The fluid density at the observation wells (ρ) is computed by:

$$\rho_m(C) = \frac{\partial \rho}{\partial C} \times C_m + \rho_f \quad (10)$$

where, m = number of observation wells; C = solute concentration (kg/m^3) and ρ_f = freshwater density (kg/m^3).

3.3.4. State variables

The monthly water table level (w.r.t MSL) and TDS data for the study area are obtained from 14 observation wells. The hydraulic head

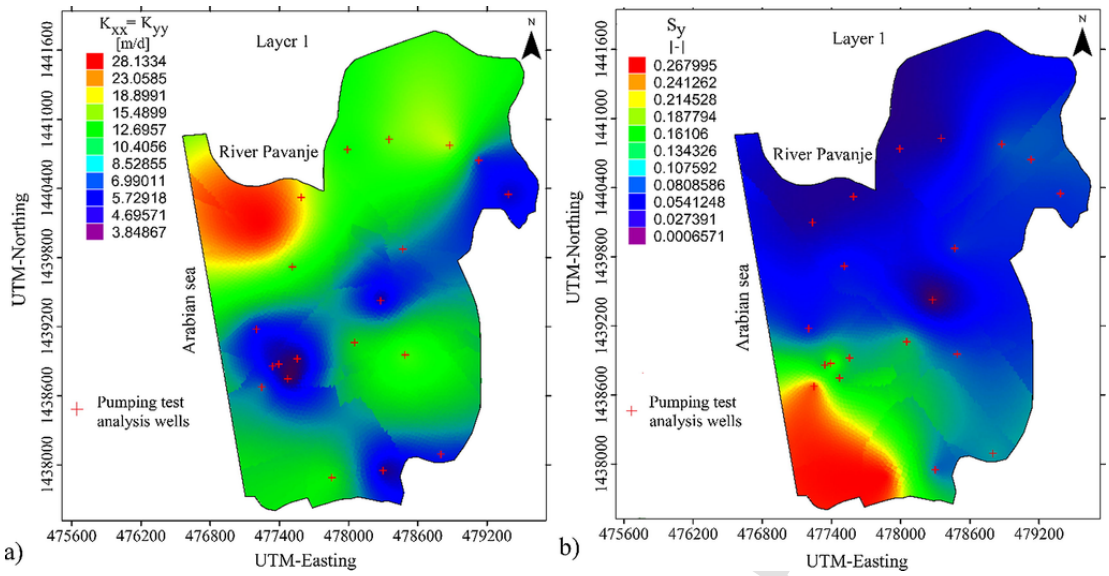

Fig. 4. Spatial distribution of (a) hydraulic conductivity (K) and (b) specific yield (S_y) at layer 1.

Table 2
Layerwise aquifer parameter values.

Layer	Hydraulic conductivity (m/d)			Specific Yield, S_y	Porosity, ε (%)
	K_{xx}	K_{yy}	K_{zz}		
1	Refer Fig. 4a	$K_{xx} = K_{yy}$	$0.53K_{xx}$	Refer Fig. 4b	29–39
2	25	5.53	$0.53K_{xx}$	5–10%	35–60
3	25	25	$0.1K_{xx}$	2–4%	5–30
4	25	10	$0.1K_{xx}$	2–4%	5–50
5	25	10	$0.1K_{xx}$	2–4%	5–30

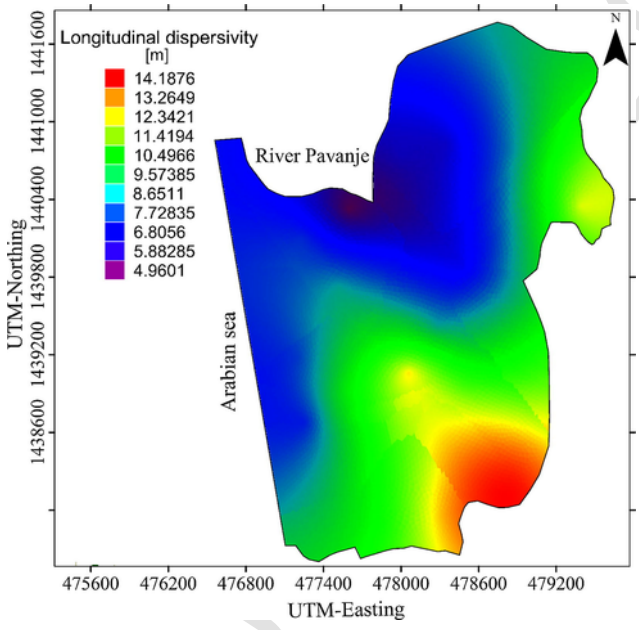

Fig. 5. Spatial distribution of the longitudinal dispersivity (α_L).

for the wells is calculated with respect to the datum and corresponding elevation above MSL. The wells 1, 4, 6, 7, 8, 11 and 12 which are located ≤500 m from the water bodies show solute concentration values >0.25 kg/m^3, but in well 2, which is located ≤250 m from the water body (Fig. 1b) the temporal concentration values <100 mg/L. This indicates that the solute concentration data in the locality is not consistent; this is because of other sources contaminating the well water. The depth at which the water is sampled for TDS analysis is not available. According to the World Health Organization (WHO), the acceptable TDS value for drinking water is below 0.5 kg/m^3, therefore TDS values >0.5 kg/m^3 are only considered.

Table 3
Other input parameters for the numerical model.

Quantity	Symbol	Value	Unit
Molecular diffusion coefficient	D_m	0.0000864	m^2/d
Freshwater density	ρ_f	1000	kg/m^3
Seawater density	ρ_s	1025	kg/m^3
Dynamic viscosity of fluid	μ	280985.76	kg/m/yr

3.4. Application of inverse modeling

The first step is to identify whether the given hydro-geological parameters of the developed conceptual model are accurate or not. This can be done by the model evaluation (discussed in Section 3.4.1) with respect to the observed state variables. As discussed in the previous section, the TDS values <0.5 kg/m^3 (500 mg/L) are not considered for the study, therefore the model performance for solute concentration is evaluated for the wells 7 and 11 only, for a period of 3 years. The next step is to identify the important parameters for understanding the dynamics between groundwater flow and SWI based on model evaluation and literature.

The significant parameters are estimated using the inverse model without changing the other model inputs. For minimizing the solute concentration term (C) in Eq. (3), TDS values for all the 14 observation

wells over 3 years are considered. The aquifer parameters to be estimated are parameterized with pilot points (parameter adjustable/computational points). The pilot points are randomly spaced with an equal number of points in each layer and the spacing between these points are based on Monte Carlo sampling with 5 iterations (Fig. 6). The parameters estimated at the pilot points are interpolated using Kriging to get the continuous function of the spatial variability. The measure of location and variability of the estimated heterogeneous aquifer parameter values in each layer is characterized by μ, σ, geometric mean (GM), median, maximum and minimum parameter value, skewness (a measure of symmetry), and Kurtosis (a measure of peakedness). Box–and–Whisker figure is plotted to graphically represent μ, σ, geometric mean (GM), median, maximum and minimum parameter value. The histogram is an effective graphical representation to indicate the skewness and Kurtosis of the data set. For further details on skewness and Kurtosis, the readers can refer to Das (2009).

The inverse calibrated model is validated over a period of two years with the water level data, measured twice in a month, at four validation wells (Honnanagoudar, 2014). These validation wells are different from the observation wells considered for the parameter estimation. Since the adequate solute concentration data is not available at the validation wells, the validation is only for the hydraulic head. The electrical resistivity measurements carried out by IRD and NITK during January/February 2008 are used to validate the simulated TDS values. The inverted ERT results provide continuous subsurface characterization and are used for validation. The numerical model results on solute concentration are validated with equivalent solute concentration derived from inverted ERT (Hoareau, 2009). The following Eq. (11) given by Comte and Banton (2007) provide the relation between pore water conductivity (in μS/cm) and solute concentration (TDS) (in mg/L).

$$\sigma_w = 2.211(\mathrm{TDS})^{0.926} \tag{11}$$

The pore water conductivity (σ_w) and bulk electrical conductivity (σ) are expressed linearly (Archie, 1942; Comte and Banton, 2007) as:

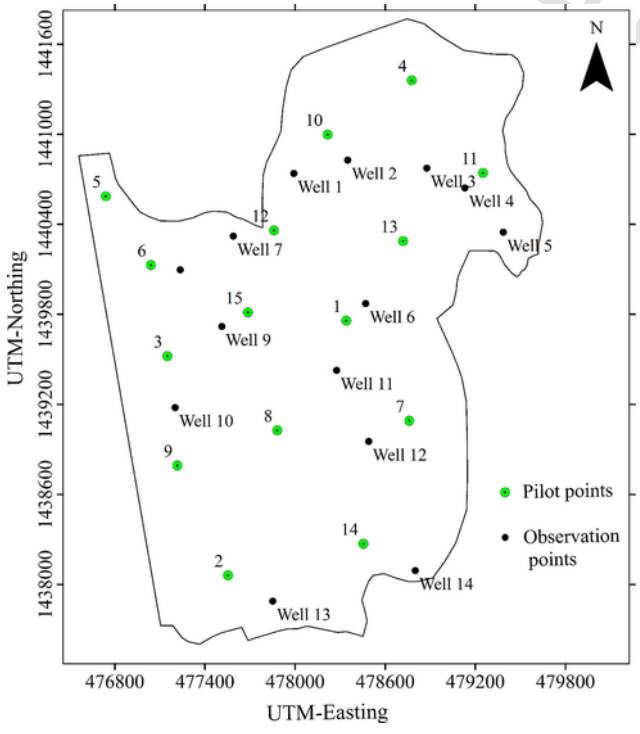

Fig. 6. Randomly spaced pilot points based on Monte Carlo sampling.

$$\sigma = \sigma_w \frac{n^m}{a} \tag{12}$$

where, n = total matrix porosity = 0.45–0.5 for the present study, a = coefficient of pore tortuosity = 1, and m = cementation factor = 1.3–2.0 (Archie, 1942). From the above relationships, the equivalent TDS values are derived from the electrical resistivity data and are used to validate the simulated TDS values.

3.4.1. Model evaluation

The performance of the model is evaluated by Root Mean Square Error (RMSE), bias error (b) and coefficient of determination (R2).

$$\mathrm{RMSE}^{\mathrm{temporal}} = \sqrt{\left(\frac{\sum_{t=1}^{n}\left([e_t]_i\right)^2}{n}\right)} \tag{13}$$

$$\mathrm{RMSE}^{\mathrm{spatial}} = \sqrt{\left(\frac{\sum_{i=1}^{m}\left([e_i]_t\right)^2}{m}\right)} \tag{13a}$$

$$\mathrm{b} = \frac{\sum_{t=1}^{n}\left([e_t]_i\right)}{n} \tag{14}$$

$$\mathrm{R}^2 = \left(\frac{\mathrm{cov}(s_t, s_t^*)}{\sigma_t \times \sigma_t^*}\right)^2_i \tag{15}$$

where, e = error between simulated and observed values of state variables; s = simulated state variable; s^* = observed state variable and cov = covariance. The $R^2 > 0.6$ is considered to be a good fit in hydrological modeling (Moriasi et al., 2007; Lathashri and Mahesha, 2015).

From the forward modeling results and the earlier studies (e.g., Sanz and Voss, 2006; Abarca et al., 2007; Ataie-Ashtiani et al., 2013) hydraulic conductivity and dispersivity are the two significant parameters to assess SWI. Therefore, inverse modeling is used to estimate major axes anisotropic heterogeneous hydraulic conductivity and heterogeneous longitudinal dispersivity. In this study, hydraulic conductivity in the z-direction is not as important as K_{xx}, K_{yy} and α_L because the geological formation below layer 2 is mostly laterite with/without the presence of clay or fissured zone. In such a case, the harmonic mean of hydraulic conductivity in a layer will be small; thus, K_{zz} is not evaluated.

4. Results and discussion

4.1. Developed conceptual model

The developed conceptual model is simulated for 3 years (number of temporal observation = 37) with a stress period of 1 day. The mean $\mathrm{RMSE}_h^{\mathrm{temporal}}$ (temporal RMSE of the hydraulic head) and mean temporal b_h (b of the hydraulic head) of 14 observation wells over 3 years are 2.56 m and −2.182 m, respectively, indicating that the simulated values are less than the observed. The mean temporal R_h^2 (R^2 of the hydraulic head) value over 14 observation wells is 0.505 (< 0.6), which indicates poor fit between the observed and simulated hydraulic heads. Fig. 7 illustrates the $\mathrm{RMSE}_h^{\mathrm{spatial}}$ (spatial RMSE for the hydraulic head) for 37 temporal observations over 14 observation wells and the value ranges between 3.55 m (May 2005) and 5.5 m (July 2007). The $\mathrm{RMSE}_h^{\mathrm{spatial}}$ = 4.96 m for the monsoon period and $\mathrm{RMSE}_h^{\mathrm{spatial}}$ = 4.21 m for the non-monsoon period. High $\mathrm{RMSE}_h^{\mathrm{spatial}}$ and low R_h^2 indicates that the misfit between the simulated and observed hydraulic heads are high and poorly correlated. Even though layer 1 of the conceptual model is considered spatially varying (Fig. 4), the performance of the

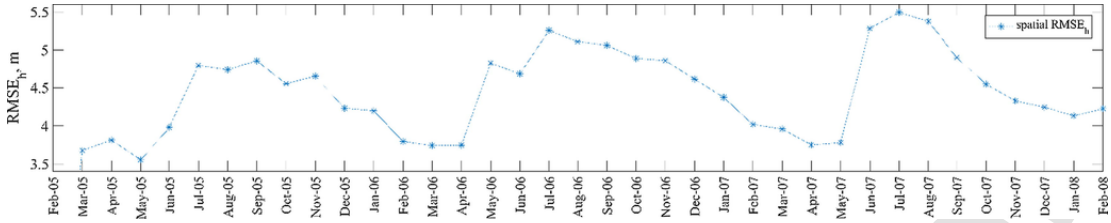

Fig. 7. Spatial RMSE$_h$ of the developed conceptual model.

model is poor; this suggests that the hydraulic head is dependent on the heterogeneity of the other layers. The storage term does not influence the hydraulic head significantly over a simulation time of one day. Thus, it can be concluded that the hydraulic conductivity is a deterministic parameter in the modeling of the hydraulic head.

The $RMSE_C^{temporal}$ (temporal RMSE of the solute concentration) at wells 7 and 11 are 0.42 kg/m^3 and 0.721 kg/m^3, respectively, and temporal b_C (b of the solute concentration) at wells 7 and 11 are −0.368 kg/m^3 and −0.717 kg/m^3, respectively. The temporal R_C^2 (R^2 of the solute concentration) at well 7 and 11 are 0.193 and 0.482, respectively, which indicates poor fit between the observed and simulated solute concentrations. Thus, it can be concluded that the errors in the solute concentration values are mainly due to the homogeneous solute transport parameters. According to the literature, dispersivity is one of the important parameters in assessing SWI (Sanz and Voss, 2006; Abarca et al., 2007; Ataie-Ashtiani et al., 2013). From the model evaluation and the literature, it can be concluded that the anisotropic spatially varying hydraulic conductivity and dispersivity are the two deterministic parameters in the modeling of the SWI.

4.2. Inverse modeling

The optimal fit between the simulated and observed state variables are estimated by finding a set of anisotropic hydraulic conductivity and longitudinal dispersivity values. A total of 1134 data points are used for the inverse modeling, i.e., 44 temporal observed values on the hydraulic head and 37 temporal observed values on the TDS at each observation well. There are 75 pilot points in a 5 layered-model, and three parameters i.e., K_{xx}, K_{yy}, and α_L are estimated at each pilot point. A single iteration of the optimization requires approximately 160 h to estimate 225 values (K_{xx}, K_{yy}, and α_L) on the 64-bit pathway, a 3.07 GHz processor and 12.0 GB of RAM. From the 4th iteration, only K_{xx} and K_{yy} parameters are considered, since the relative change in α_L values are ≤0.1 and time taken is reduced to approximately 71 h on the same configuration machine. Hence, approximately 1620 h are required for the inverse model to terminate and the termination criterion is $\frac{\Phi_i - \Phi_{min}}{\Phi_i} \leqslant 0.1$. The estimated parameters from the inverse model are discussed in the following sections.

4.2.1. Hydraulic conductivity

The statistics of the estimated hydraulic conductivities in *x* and *y* major axes are summarized in Fig. 8a and 8b, respectively. The layerwise spatial variability of the hydraulic conductivity in *x* and *y* major axes are shown in the Figs. 9 and 10, respectively, along with the histograms.

From Fig. 8a, it is observed that the overall hydraulic conductivity values along the *x* major axis range from 0.374 to 63.221 m/d. From Fig. 9, it can be noticed that the K_{xx} values along the coastal length (near the sea) are <3.5 m/d in layers 2 and 5, indicating the existence of a less permeable geological formation. Based on Table 1, the following interpretations of the soil composition have been made. Layer 1 has 30.94% of coastal alluvium, 47.91% of lateritic clay and 21.15% of laterite soil. Layer 2 has 60.75% of clayey sand or fine silt, 9.87% of laterite soil and 29.38% of fissured rock/lateritic clay. Layer 3 has 52.08% of clay and silt formation, 10.48% of weathered zone and 37.44% of fissured rock/lateritic clay. Layer 4 has 46% of clay and silt formation, 50.81% of fissured bedrock and remaining of weathered bedrock. Layer 5 has 35.58% of clay/silt zone, 20.4% of weathered bedrock and 44.02% of the fissured rock.

From Fig. 10, the K_{yy} values range from 0.53 to 30 m/d, which is not similar to that of K_{xx} range because of the upper limit (p_j^u) in Eq. (3a) for K_{yy} was assigned a value of 30 m/d. This difference is due to

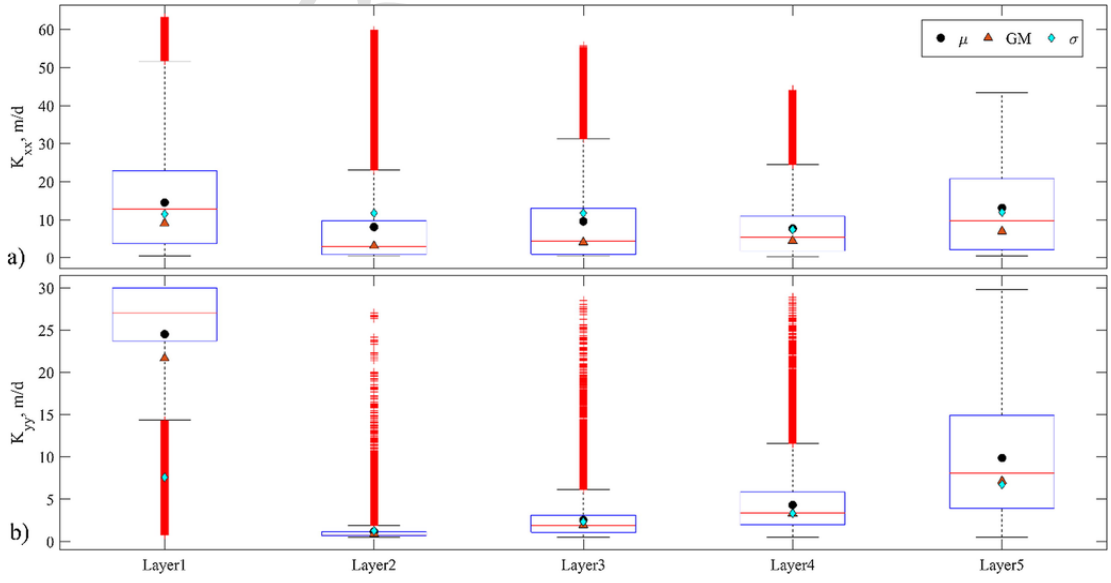

Fig. 8. Box–and–Whisker plot to summarize the statistics of the hydraulic conductivities in each layer, (a) in *x* major axis and (b) in *y* major axis.

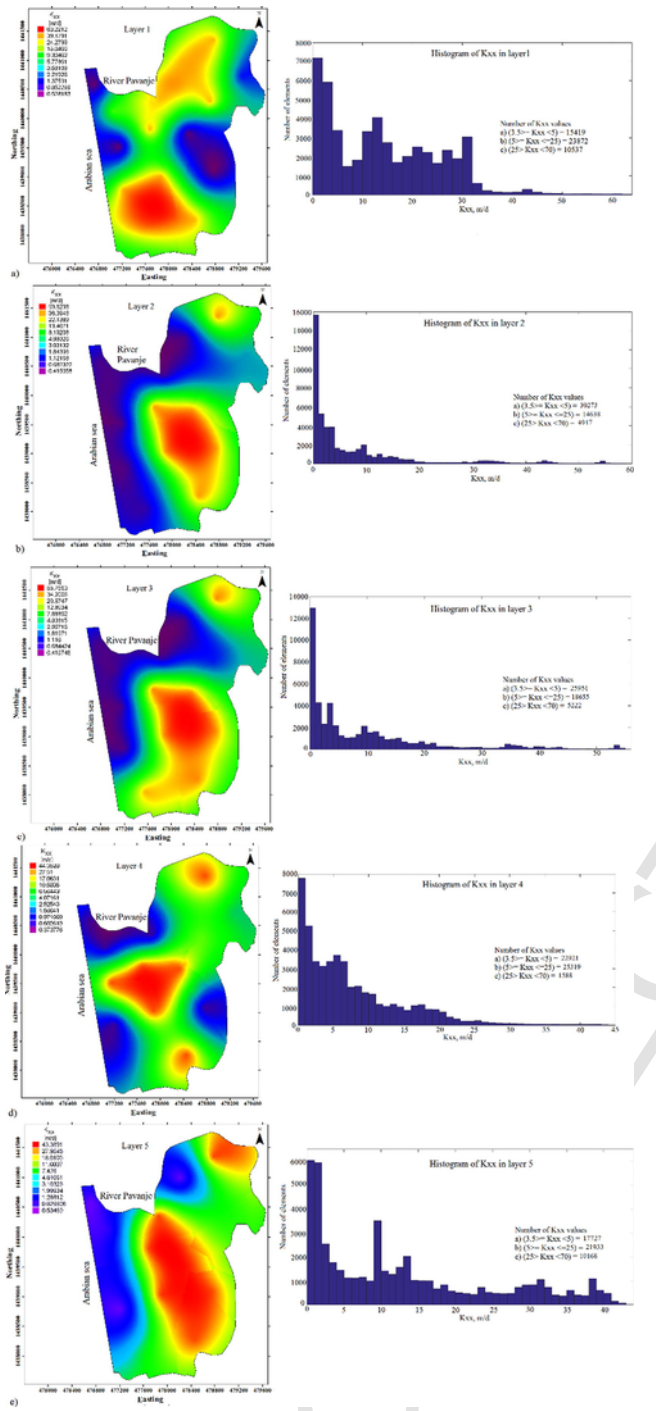

Fig. 9. Layerwise spatial distribution of K_{xx} and the respective histogram (a) layer 1, (b) layer 2, (c) layer 3, (d) layer 4 and (e) layer 5.

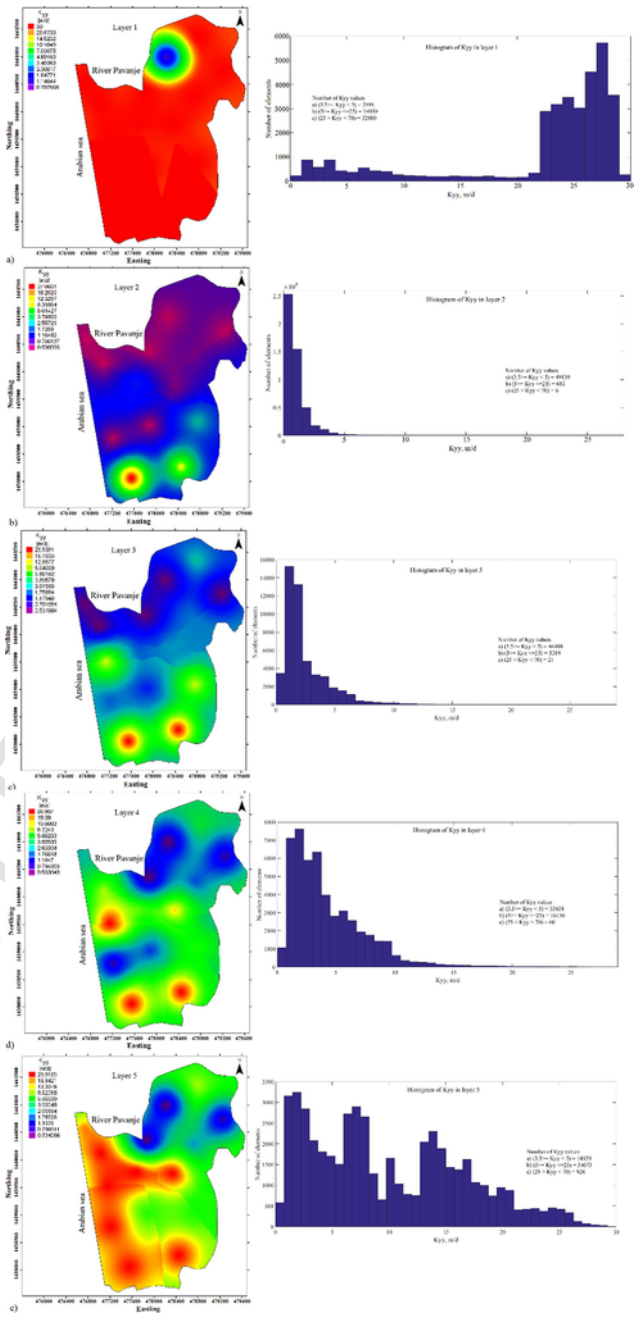

Fig. 10. Layerwise spatial distribution of K_{yy} and the respective histogram (a) layer 1, (b) layer 2, (c) layer 3, (d) layer 4 and (e) layer 5.

groundwater flow to the sea along the *x*-direction. From the histograms of K_{yy} and Table 1, the soil type parallel to the coast can be interpreted as in layer 1, 65.83% of elements are laterite soil out of which 47.9% for elements have the K_{yy} value = 30 m/d, 28.16% of lateritic clay and remaining is covered with coastal alluvium. Layer 2 is a homogeneous layer since 98.62% is clay/silt formation. Layer 3 has 89.3% of clay and silt formation, and remaining is fissured bedrock/lateritic clay. Layer 4 has 67.51% of clay and remaining is fissured bedrock. Layer 5, fissured bedrock covers 68.38%, 29.76% of clay/silt zone and remaining with a small amount of weathered bedrock. From this, it can be concluded that the layers parallel to the coast have no or thin layer of weathered bedrock (also evident from Fig. 2).

4.2.2. *Dispersivity*

The spatial distribution and statistics of the estimated α_L at layer 1 are shown in Fig. 11a and 11b, respectively. Fig. 11c is the histogram of the estimated α_L. From Fig. 11a, it is observed that the α_L values vary between 6.265 and 11.901 m. At the wells 1, 2, 6 and 8 the $\alpha_L < 7.5$ m, at the wells 7, 9 and 10 the α_L ranges between 7.5 and 9 m and at remaining wells the $\alpha_L > 9$ m. The spatial distribution of α_L in other layers are same as shown in the Fig. 11a. The Fig. 11d shows the comparison between α_L values estimated from the Xu & Eckstein formula and the inverse model. The wells 5 and 14 are not considered because $L > 1$ km from the source and the rate of increase of dispersivity be-

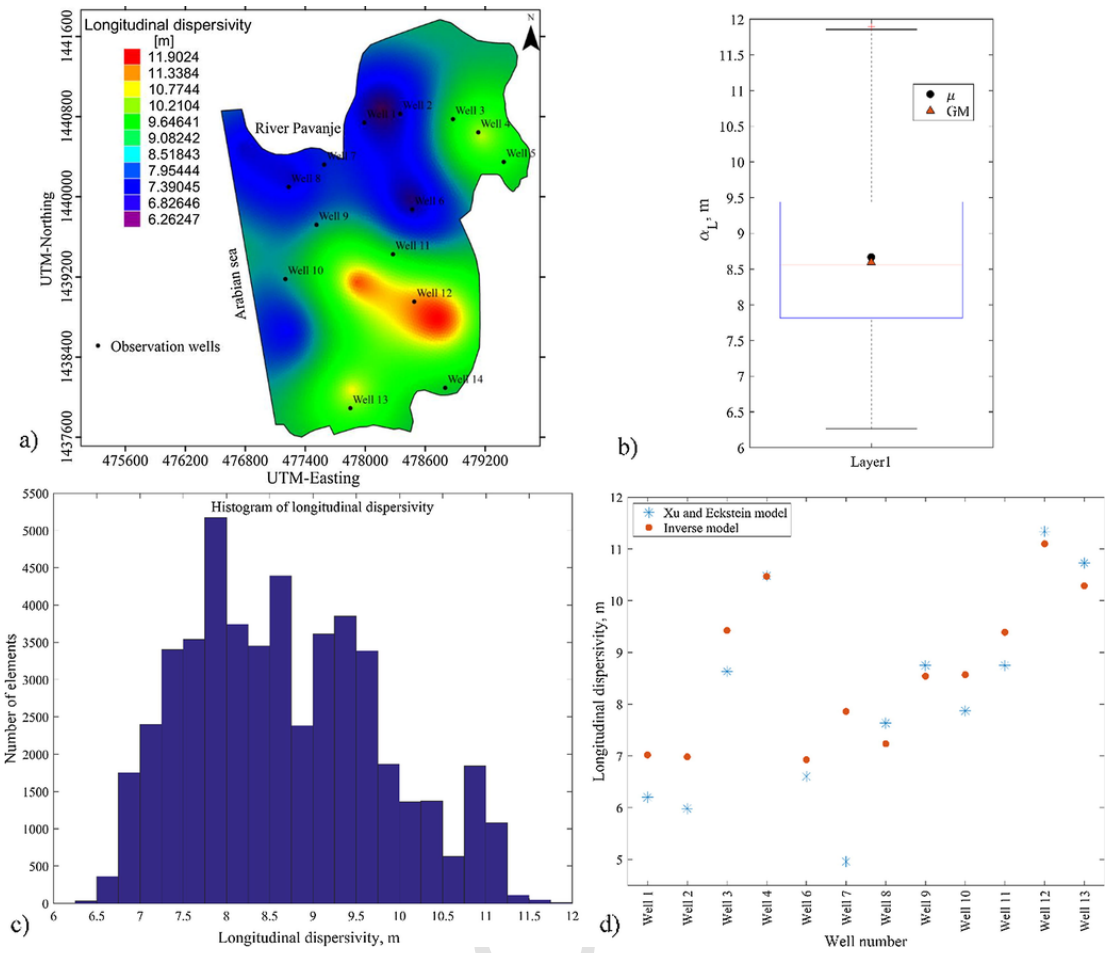

Fig. 11. (a) Spatial distribution, (b) Box–and–Whisker plot to summarize the statistics, (c) histogram of the estimated α_L in layer 1 and (d) comparison of the inverse model with the Xu & Eckstein formula.

yond 1 km can be neglected (Xu and Eckstein, 1995). At the well 4, the α_L value from the inverse model exactly coincides with the α_L value derived by the regression formula. At wells 6, 8, 9, 12 and 13, the α_L values of the inverse model and from the regression equation are approximately the same.

4.2.3. *Inverse calibrated model performance*

The temporal performance of the inverse calibrated model over time is evaluated by using R_h^2, b_h and $RMSE_h$ (Table 4). The negative sign of *b* indicates that the inverse calibrated model underestimates the state variables and vice versa. From Table 4, it is observed that the mean temporal R_h^2 (R^2 of the hydraulic head) of the inverse calibrated model for the 14 observation wells over 3 years has improved by 1.64 times than the developed conceptual model, which indicates better and improved fit between the observed and the simulated hydraulic heads. The mean temporal b_h (b of the hydraulic head) and mean $RMSE_h^{temporal}$ (temporal RMSE of the hydraulic head) of the inverse calibrated model for the 14 observation wells over 3 years decreased by 75.7% and 50.8%, respectively from the developed conceptual model. Fig. 12, illustrates the monthly $RMSE_h^{spatial}$ (spatial RMSE for the hydraulic head) over 14 observation wells. The $RMSE_h^{spatial}$ has reduced by 64% for both the monsoon and non-monsoon period when compared with the developed conceptual model.

Table 4
Comparison between the temporal performance of the developed conceptual and the inverse calibrated model.

Temporal performance measure for the hydraulic head	Mean R_h^2	Mean b_h (m)	Mean $RMSE_h$ (m)
Developed conceptual model	0.505	−2.182	2.563
Inverse calibrated model	0.828	−0.53	1.262
Temporal performance measure for the solute concentration	R_C^2	b_C (kg/m^3)	$RMSE_C$ (kg/m^3)
Developed conceptual model at well 7	0.193	−0.368	0.42
Inverse calibrated model at well 7	0.093	−0.333	0.396
Developed conceptual model at well 11	0.482	−0.717	0.721
Inverse calibrated model at well 11	0.551	−0.655	0.657

From Table 4, it can be observed that the temporal R_C^2 improves in well 11 from 0.482 to 0.551, but the fit between the observed and simulated concentrations at well 7 is still poor. This discrepancy may be because of the influence of the contaminated river on the adjacent observation well 7. The $RMSE_C^{temporal}$ at wells 7 and 11 reduced by 5.7% and 8.87%, respectively, and temporal b_C at wells 7 and 11 reduced by 9.5%. The reduction in errors of solute concentration is not >10% indicating the additional data requirement for the calibration.

4.3. *Validation and verification*

4.3.1. *Validation of the inverse calibrated model for the hydraulic head*

The model efficiency of the inverse calibrated model at each validation well is tabulated (Table 5). Since there are only 4 wells, the performance of the inverse calibrated model is validated only at well points

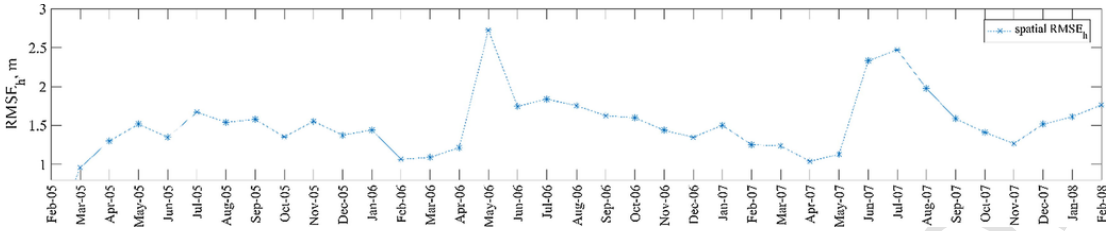

Fig. 12. Spatial RMSE$_h$ of the inverse calibrated model.

Table 5
Temporal performance of the inverse calibrated model at the validation wells.

Validation well no.	Temporal R_h^2	Temporal b_h (m)	Temporal RMSE$_h$ (m)
V1	0.610	1.391	1.647
V2	0.643	2.293	2.451
V3	0.800	0.089	0.302
V4	0.903	0.202	0.329

and not spatially. The goodness of fit between the observed and simulated hydraulic heads are >0.6, which indicates a good fit. Fig. 13 compares the hydraulic head between the observed and simulated values. The validation wells V3 and V4, which are located near the river (Fig. 1b) show good correlation, which indicates that the given boundary condition for the river is accurate. From Fig. 13, it can be noticed that at wells V1 and V2 there is a sudden increase in the observed hydraulic head of >3 m at the beginning of the monsoon, which indicates that the requirement of the field investigation to understand this sudden change in the hydraulic head.

4.3.2. Validation of the inverse calibrated model for the solute concentration

Fig. 14a shows ERT at profile L1 (refer Fig. 1b); these resistivity values are converted into equivalent TDS values (Fig. 14b) using Eq. (11) and Fig. 14c represents the results of solute transport by the inverse calibrated model. The results of the numerical model (Fig. 14c) are validated with the equivalent TDS values (Fig. 14b). It can be observed that, in Fig. 14b and c, at −5 m (below MSL), the TDS values are >1500 mg/L, indicating the maximum intrusion at the same depth. The resistivity values of the saturated clay and silt formation vary between 30 and 80O-m (refer to Table 1). It is known that Archie's law is not valid in the presence of clay formation; thus the clay formation cannot be considered as SWI at 170–270 m (Fig. 14b).

To quantify the error in the simulated TDS values, the electrical resistivity data points are matched with the simulated TDS data points based on the Euclidean distance. The data points with a Euclidean distance >1 m are not considered for the model evaluation (Fig. 15a). From the Fig. 15a, the bias error between the equivalent and simulated TDS values mostly lie between −0.2–0.2 kg/m^3. Fig. 15b illustrates the goodness of fit between the equivalent and simulated TDS values. The RMSE and b are 0.213 kg/m^3 and −0.078 kg/m^3, respectively, implying the confidence in the inverse calibrated model results. The validation method adapted here is novel and is used to quantify the error between the measured and simulated results.

4.3.3. Verification of layering and geological formation

The estimated hydraulic conductivity in *x* and *y* directions are verified for layering and geological formation (Table 1), i.e., by comparing the vertical 2D profile from the inverse calibrated model with ERT image (Fig. 16). For this verification, the profiles T1 and L2 are considered, such that they are located >1 km from the coastal line (Fig. 1b) and these profiles are not subjected to SWI. In the profile T1 (Fig. 16a), it is noticed that an average of 9 m thick saturated clayey formation is in between −1 m and −8 m and from the inverse calibrated model output, 7 m thick saturated clayey formation on an average is found in between 2 m and −6 m. In the profile L2 (Fig. 16b), it is seen that the inverse calibrated model can reproduce the clayey formation between 470 and 540 m distance. The homogeneous pattern of the weathered zone can be noticed in the 2D sections of ERT image and the inverse calibrated model result (Fig. 16b). From this observation, it can be concluded that the interpolated layer thickness and the estimated geological formation is similar to the field measurements.

The parameter estimation approach at pilot points by using highly parameterized inverse model offers guidance on estimating anisotropic heterogeneous hydraulic conductivity and dispersivity in real-field layered unconfined aquifer involving SWI. The use of real-field data such as appropriate initial aquifer parameters and constraining the inverse

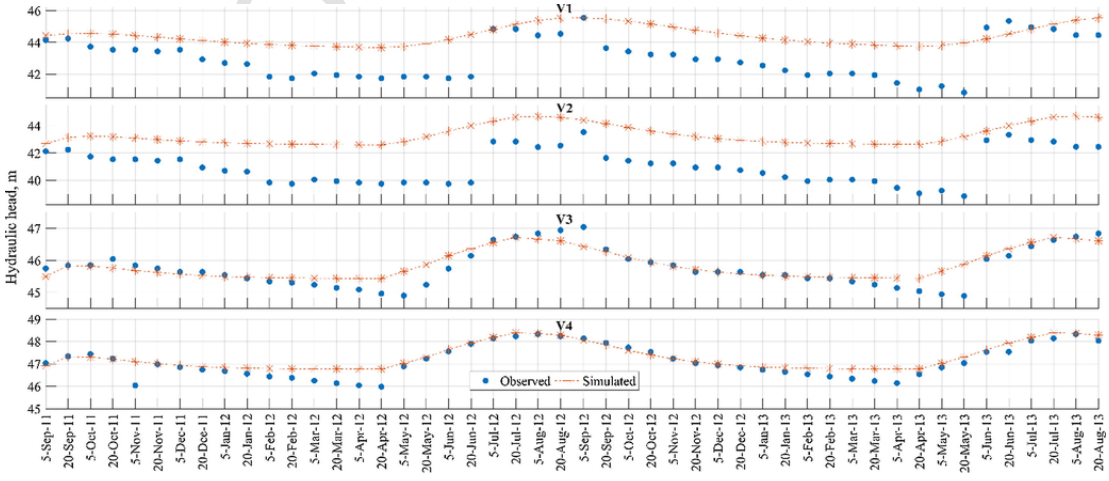

Fig. 13. Comparison between the observed hydraulic head (dots) and simulated hydraulic head (asterisks with dash line) at each validation well.

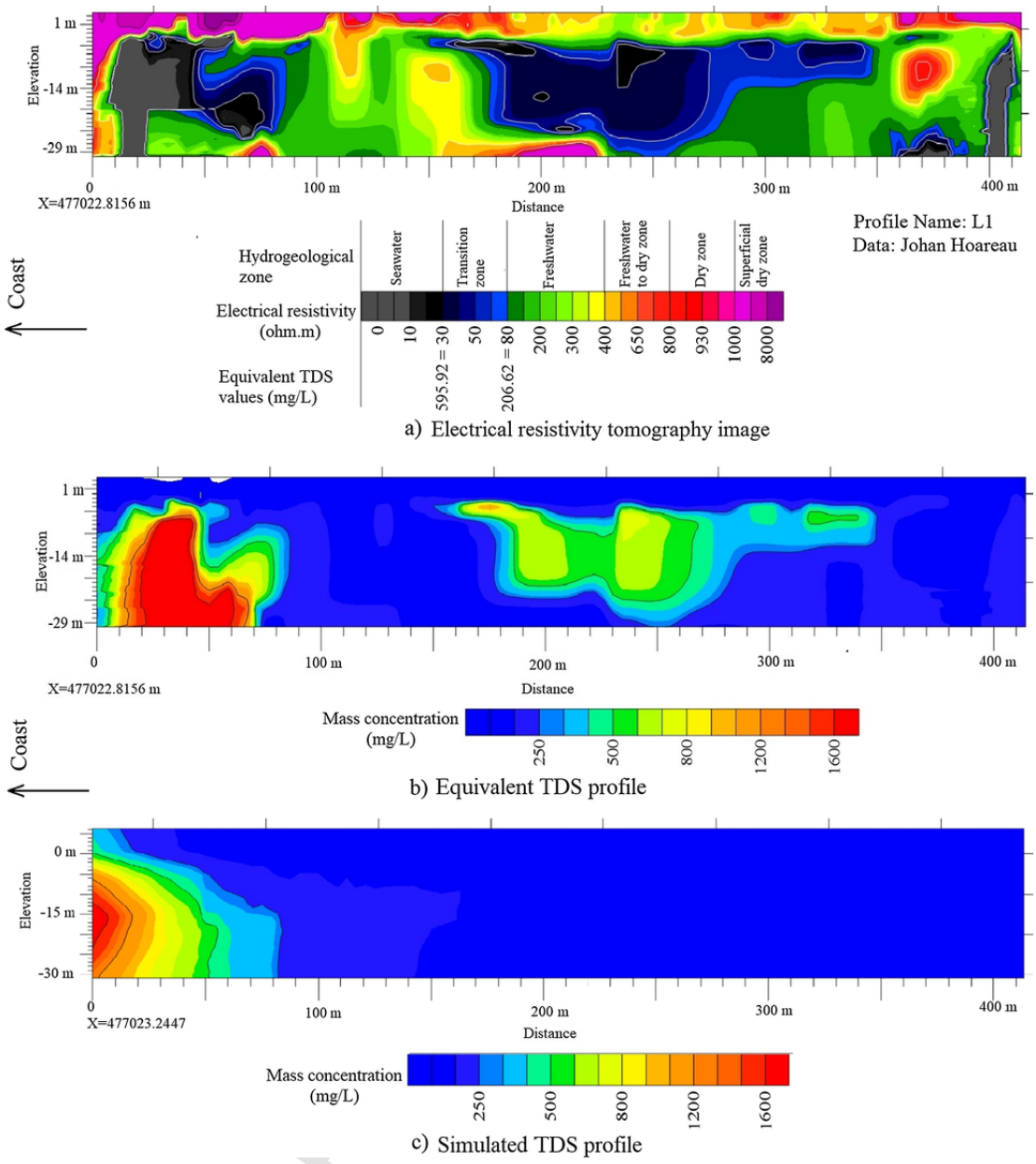

Fig. 14. Comparison validation of a simulated SWI profile; (a) ERT image, (b) calculated equivalent TDS profile, and (c) inverse calibrated model simulated TDS profile.

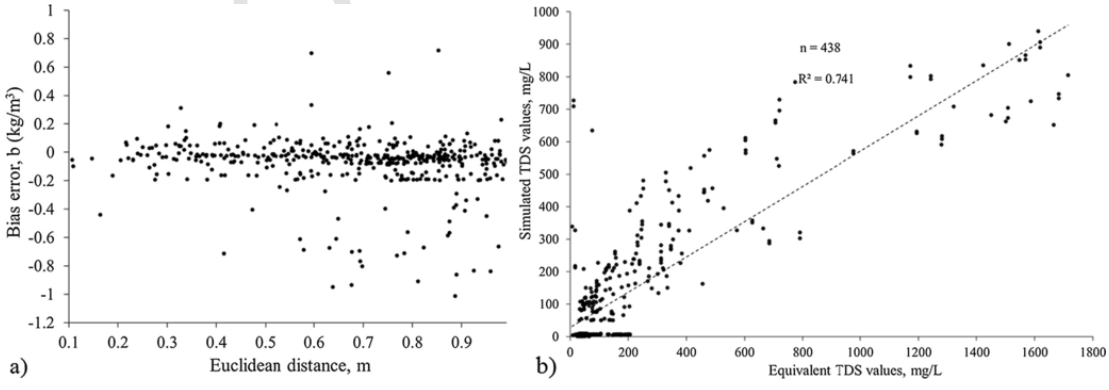

Fig. 15. Scatter plot between the equivalent and simulated TDS; (a) bias error with respect to Euclidean distance and (b) R^2 fit.

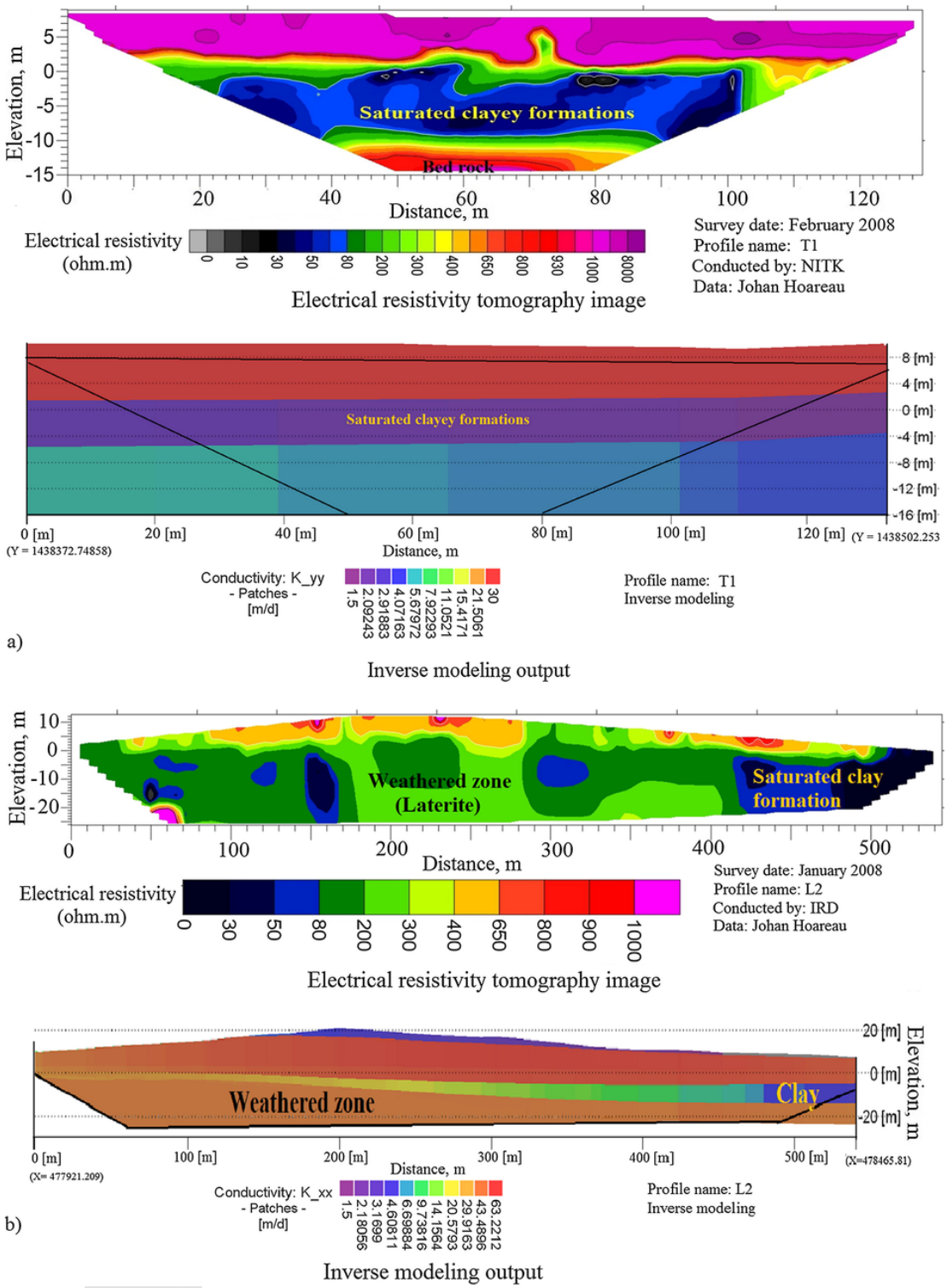

Fig. 16. Verification of the geological formation with ERT image; (a) profile T1 and (b) profile L2.

model with the upper and lower bounds of the parameters reduces the number of iterations required to minimize the objective function, improve the potential estimates and possible convergence. The inverted electrical resistivity output used for validation significantly supports the methodology adopted for the inverse modeling.

5. Summary and conclusions

In this study, a 3D variable-density, unconfined coastal aquifer model is developed by constraining the model with aquifer topography and appropriate initial field conditions. From the forward modeling results, it is observed that the anisotropic spatially varying hydraulic conductivity and dispersivity are the deterministic parameters to assess the

SWI in a coastal aquifer. The inverse code (PEST) is used to minimize the least-square error for the state variables and to estimate these deterministic parameters. A reliable validation method is adopted to evaluate the inverse calibrated model results with the ERT profile. The aquifer layering and the estimated geological formation are verified by comparing with ERT images. The study explains the necessity of considering layering and anisotropic heterogeneous aquifer parameters for effective simulation of SWI. The analysis gives knowledge about the geological formation in the study area. The present study infers the following points:

- The low performance of the developed conceptual model signifies the importance of considering spatially varying aquifer flow and solute transport parameters in all the layers. The high error in the hydraulic head indicates that the hydraulic conductivity is one of the deterministic parameters since storage term does not influence the hydraulic head significantly over a simulation time of one day.
- The inverse model used to estimate anisotropic spatially varying hydraulic conductivities and heterogeneous longitudinal dispersivity is computationally demanding, but this effort is worthwhile to obtain the spatially varying aquifer parameters.
- The inverse calibrated model results show substantial improvement; error in the hydraulic head is reduced by >50% when compared with the developed conceptual model. The error in the solute concentration is reduced by 10% (which suggests additional data requirement).
- Though the least square error of the state variables is minimized at the observation wells, the validation of the inverse calibrated model shows good results at the validation wells, which significantly support the performance of the inverse calibrated model.
- The TDS values determined by the inverse calibrated model is evaluated with equivalent TDS values computed from the electrical resistivities. The inverse calibrated model results show better agreement with the field data and a novel validation method adapted is more reliable than the commonly used comparison validation.
- The comparison verification of layering shows good agreement with the electrical resistivities layers. The verification also shows that the inverse calibrated model is able to reproduce the field data.
- The knowledge of geological formation, normal and parallel to the coast has improved based on the estimated anisotropic heterogeneous hydraulic conductivity, which can be used for the planning strategies and management of the aquifer system.

Acknowledgments

The authors thank Johan Hoareau, Jean-Michel Vouillamoz (University Grenoble Alpes, IRD, CNRS, Grenoble INP, IGE, CS407000, 38058 Grenoble CEDEX 9, France) for sharing the geophysical data and Laurent Ruiz, Indo-French Cell for Water Sciences, IISc, Bangalore. The authors would like to thank the anonymous reviewers for their valuable suggestions and constructive comments. This research did not receive any specific grant from funding agencies in the public, commercial, or not-for-profit sectors.

Appendix A. Supplementary data

Supplementary data associated with this article can be found, in the online version, at https://doi.org/10.1016/j.jhydrol.2018.08.031.

References

Abarca, E., Carrera, J., Sanchez-Vila, X., Dentz, M., 2007. Anisotropic dispersive Henry problem. Adv. Water Resour. 30 (4), 913–926.

Abarca, E., Vázquez-Suñé, E., Carrera, J., Capino, B., Gámez, D., Batlle, F., 2006. Optimal design of measures to correct seawater intrusion. Water Resour. Res. 42 (9), W09415.

Alcolea, A., Carrera, J., Medina, A., 2006. Pilot points method incorporating prior information for solving the groundwater flow inverse problem. Adv. Water Resour. 29 (11), 1678–1689.

Archie, G.E., 1942. The electrical resistivity log as an aid in determining some reservoir characteristics. Trans. AIME 146 (01), 54–62.

Ataie-Ashtiani, B., Rajabi, M.M., Ketabchi, H., 2013. Inverse modelling for freshwater lens in small islands: Kish Island. Persian Gulf. Hydrol. Process. 27 (19), 2759–2773.

Bastani, M., Kholghi, M., Rakhshandehroo, G.R., 2010. Inverse modeling of variable-density groundwater flow in a semi-arid area in Iran using a genetic algorithm. Hydrogeol. J. 18 (5), 1191–1203.

Beaujean, J., Nguyen, F., Kemna, A., Antonsson, A., Engesgaard, P., 2014. Calibration of seawater intrusion models: inverse parameter estimation using surface electrical resistivity tomography and borehole data. Water Resour. Res. 50 (8), 6828–6849.

Bhosale, D.D., Kumar, C.P., 2001. Simulation of seawater intrusion in Ernakulam coast. (http://www.angelfire.com/nh/cpkumar/publication/ernac.pdf Retrieved November 13, 2017).

Bray, B.S., Tsai, F.T.-C., Sim, Y., Yeh, W.W.G., 2007. Model development and calibration of a saltwater intrusion model in southern California. JAWRA 43 (5), 1329–1343.

Carrera, J., 1988. State of the art of the inverse problem applied to the flow and solute transport equations. In Groundwater flow and quality modelling. Springer, Dordrecht, 549–583.

Carrera, J., Hidalgo, J.J., Slooten, L.J., Vazquez-Sune, E., 2010. Computational and conceptual issues in the calibration of seawater intrusion models. Hydrogeol. J. 18, 131–145.

Cobaner, M., Yurtal, R., Dogan, A., Motz, L.H., 2012. Three dimensional simulation of seawater intrusion in coastal aquifers: A case study in the Goksu Deltaic Plain. J. Hydrol. 464–465, 262–280.

Comte, J.C., Banton, O., 2007. Cross-validation of geo-electrical and hydrogeological models to evaluate seawater intrusion in coastal aquifers. Geophys. Res. Lett. 34 (10).

Cooley, R.L., 1977. A method of estimating parameters and assessing reliability for models of steady state groundwater flow: 1. Theory and numerical properties. Water Resour. Res. 13 (2), 318–324.

Das, N.G., 2009. Statistical methods. Tata. McGraw-Hill Publishing Company Limited, 224–244.

Dausman, A.M., Doherty, J., Langevin, C.D., 2010. Hypothesis testing of buoyant plume migration using a highly parameterized variable-density groundwater model at a site in Florida, USA. Hydrogeol. J. 18, 147–160.

Diersch, H.-J., G., 2014. FEFLOW: Finite element modeling of flow, mass and heat transport in porous and fractured media. Springer Science & Business Media.

Ding, F., Yamashita, T., Lee, H.S., Pan, J., 2014. A modeling study of seawater intrusion in the Liao Dong Bay coastal plain, China. J. Mar. Sci. Technol. 22 (2), 103–115.

Doherty, J., 2004. PEST Model-Independent Parameter Estimation, User Manual, 5th Edition Watermark Numerical Computing, Australia.

Emsellem, Y., De Marsily, G., 1971. An automatic solution for inverse problem. Water Resour. Res. 7 (3), 1264–1283.

Franssen, H.H., Gómez-Hernández, J.J., 2002. 3D inverse modelling of groundwater flow at a fractured site using a stochastic continuum model with multiple statistical populations. Stoch. Env. Res. Risk Assess. 16 (2), 155–174.

Franssen, H.J.H., Gómez-Hernández, J., Sahuquillo, A., 2003. Coupled inverse modelling of groundwater flow and mass transport and the worth of concentration data. J. Hydrol. 281 (4), 281–295.

Franssen, H.H., Alcolea, A., Riva, M., Bakr, M., Van der Wiel, N., Stauffer, F., Guadagnini, A., 2009. A comparison of seven methods for the inverse modelling of groundwater flow. Application to the characterisation of well catchments. Adv. Water Resour. 32 (6), 851–872.

Freeze, R.A., Cherry, J.A., 1979. Groundwater, p. 604.

Frind, E.O., Pinder, G.F., 1973. Galerkin solution of the inverse problem for aquifer transmissivity. Water Resour. Res. 9 (5), 1397–1410.

GEC, 1997. Groundwater Resource Estimation Methodology. Report of the Groundwater Resource Estimation Committee, Ministry of Water Resources, Government of India, New Delhi.

Giacobbo, F., Marseguerra, M., Zio, E., 2002. Solving the inverse problem of parameter estimation by genetic algorithms: the case of a groundwater contaminant transport model. Ann. Nucl. Energy 29 (8), 967–981.

Hoareau, J., 2009. Utilisation d'une approche couplée hydrogéophysique pour l'étude des aquiféres - Applications aux contextes de socle et côtier sableux. Ph.D. Thesis, Université Joseph-Fourrier-Grenoble 1, Grenoble, France.

Honnanagoudar, 2014. Studies on aquifer characterization and seawater intrusion vulnerability assessment of coastal Dakshina Kannada District, Karnataka. Ph.D., thesis, Department of Applied Mechanics and Hydraulics, National Institute of Technology, Karnataka, Surathkal, India.

IMD – Monthly mean maximum & minimum temperature and total rainfall based on 2004 – 2010 data. India Meteorological Department. (www.imdpune.gov.in/ Retrieved June 06, 2016.)

Iribar, V., Carrera, J., Custodio, E., Medina, A., 1997. Inverse modelling of seawater intrusion in the Llobregat delta deep aquifer. J. Hydrol. 198, 226–244.

Keidser, A., Rosbjerg, D., 1991. A comparison of four inverse approaches to groundwater flow and transport parameter identification. Water Resour. Res. 27 (9), 2219–2232.

Ketabchi, H., Ataie-Ashtiani, B., 2015. Review: Coastal groundwater optimization - advances, challenges, and practical solutions. Hydrogeol. J. 23, 1129–1154.

Kitanidis, P.K., Vomvoris, E.G., 1983. A geostatistical approach to the inverse problem in groundwater modeling (steady state) and one-dimensional simulations. Water Resour. Res. 19 (3), 677–690.

Kolditz, O., Ratke, R., Diersch, H.J.G., Zielke, W., 1998. Coupled groundwater flow and transport: 1. Verification of variable density flow and transport models. Adv. Water Resour. 21 (1), 27–46.

Kopsiaftis, G., Mantoglou, A., Giannoulopoulos, P., 2009. Variable density coastal aquifer models with application to an aquifer on Thira Island. Desalination 237, 65–80.

Lathashri, U.A., Mahesha, A., 2015. Predictive simulation of seawater intrusion in a tropical coastal aquifer. J. Environ. Eng. ASCE, ISSN 0733-9372, D4015001.

Lu, W., Yang, Q., Martin, J.D., Juncosa, R., 2013. Numerical modelling of seawater intrusion in Shenzhen (China) using a 3D density-dependent model including tidal effects. J. Earth Syst. Sci. 122 (2), 451–465.

Mahesha, A., Vyshali, Lathashri, U.A., Ramesh, H., 2012. Parameter estimation and vulnerability assessment of coastal unconfined aquifer to saltwater intrusion. J. Hydrol. Eng. 17 (8), 933–943.

Mayer, A.S., Huang, C., 1999. Development and application of a coupled-process parameter inversion model based on the maximum likelihood estimation method. Adv. Water Resour. 22 (8), 841–853.

McLaughlin, D., Townley, L.R., 1996. A reassessment of the groundwater inverse problem. Water Resour. Res. 32 (5), 1131–1161.

Medina, A., Carrera, J., 1996. Coupled estimation of flow and solute transport parameters. Water Resour. Res. 32 (10), 3063–3076.

Moriasi, D.N., Arnold, J.G., Van Liew, M.W., Bingner, R.L., Harmel, R.D., Veith, T.L., 2007. Model evaluation guidelines for systematic quantification of accuracy in watershed simulations. Trans. ASABE 50 (3), 885–900.

Motz, L.H., Sedighi, A., 2009. Representing the coastal boundary condition in regional groundwater flow models. J. Hydrol. Eng. 14 (8), 821–831.

Murty, V.V.N., Scott, V.H., 1977. Determination of transport model parameters in groundwater aquifers. Water Resour. Res. 13 (6), 941–947.

Pool, M., Carrera, J., Alcolea, A., Bocanegra, E.M., 2015. A comparison of deterministic and stochastic approaches for regional scale inverse modeling on the Mar del Plata aquifer. J. Hydrol. 531, 214–229.

Rajabi, M.M., Ketabchi, H., 2017. Uncertainty-based simulation-optimization using Gaussian process emulation: application to coastal groundwater management. J. Hydrol. 555, 518–534.

Sanz, E., Voss, C.I., 2006. Inverse modeling for seawater intrusion in coastal aquifers: insights about parameter sensitivities, variances, correlations and estimation procedures derived from the Henry problem. Adv. Water Resour. 29 (3), 439–457.

Sherif, M., Sefelnasr, A., Javadi, A., 2012. Incorporating the concept of equivalent freshwater head in successive horizontal simulations of seawater intrusion in the Nile Delta aquifer, Egypt. J. Hydrol. 464–465, 186–198.

Strecker, E.W., Chu, W.-S., 1986. Parameter identification of a groundwater contaminant transport model. Groundwater 24 (1), 56–62.

Sujay, R.N., Deka, P.C., 2016. Influence of series of vented dam intersections on the channel processes: a case study in the pavanje river basin. ISH - Hydro 2016 International, p. 8.

Sun, N., Sun, N.Z., Elimelech, M., Ryan, J.N., 2001. Sensitivity analysis and parameter identifiability for colloid transport in geochemically heterogeneous porous media. Water Resour. Res. 37 (2), 209–222.

Udayakumar, G., 2008. Subsurface barrier for water conservation in lateritic formations. Ph.D., thesis, Department of Applied Mechanics and Hydraulics, National Institute of Technology, Karnataka, Surathkal, India.

Umari, A., Willis, R., Liu, P.L.F., 1979. Identification of aquifer dispersivities in two-dimensional transient groundwater contaminant transport: an optimization approach. Water Resour. Res. 15 (4), 815–831.

Vyshali, 2008. Studies on saltwater intrusion in the coastal D.K district. Ph.D., thesis, Department of Applied Mechanics and Hydraulics, National Institute of Technology, Karnataka, Surathkal, India.

Wagner, B.J., Gorelick, S.M., 1986. A statistical methodology for estimating transport parameters: theory and applications to one-dimensional advective-dispersive systems. Water Resour. Res. 22 (8), 1303–1315.

Wagner, B.J., 1992. Simultaneous parameter estimation and contaminant source characterization for coupled groundwater flow and contaminant transport modelling. J. Hydrol. 135 (1–4), 275–303.

Xiang, Y., Sykes, J.F., Thomson, N.R., 1992. A composite L_1 parameter estimator for model fitting in groundwater flow and solute transport simulation. Water Resour. Res. 29 (6), 1661–1673.

Xiao, Y., Gu, X., Yin, S., Shao, J., Cui, Y., Zhang, Q., Niu, Y., 2016. Geostatistical interpolation model selection based on ArcGIS and spatio-temporal variability analysis of groundwater level in piedmont plains, northwest China. SpringerPlus 5, 425.

Xu, M., Eckstein, Y., 1995. Use of weighted least-squares method in evaluation of the relationship between dispersivity and field scale. Groundwater 33 (6), 905–908.

Yao, L., Huo, Z., Feng, S., Mao, X., Kang, S., Chen, J., Xu, J., Steenhuis, T.S., 2014. Evaluation of spatial interpolation methods for groundwater level in an arid inland oasis, northwest China. Environ. Earth Sci. 71 (4), 1911–1924.